EXPERIMENTAL STUDY OF A LIGHT COMMERCIAL REFRIGERATION SYSTEM OPERATING UNDER FROSTING CONDITONS

DA SILVA D.L. [(**)], TASSOU S.A.[(*)], HADAWEY A.[(*)]
[(*)]School of Design and Engineering, Brunel University, Uxbridge, Middlesex, UB8 3PH, England,
Savvas.Tassou@brunel.ac.uk

[(**)] POLO Laboratories for Emerging Technologies in Cooling and Thermophysics
Federal University of Santa Catarina, 88040970, Florianópolis-SC, Brazil
diogo@polo.ufsc.br

ABSTRACT

This paper reports the results of investigations into the frosting process of a serve-over counter cabinet. The refrigeration system was instrumented with high accuracy transducers and tested in an environmental test chamber at controlled conditions of ambient temperature and relative humidity. Measurements of the refrigerant mass flow rate, low and high side pressures, coil surface temperature and the state point of the air upstream and downstream of the evaporator were made to assess the system performance. In addition, mass and energy balances were applied on the evaporator in order to determine the cooling capacity and the accumulated mass of frost over time. The results show the influence of ambient conditions on the system performance and how frost formation affects the measured parameters. The cooling capacity and the coil temperature were correlated, indicating the potential application of the latter variable as a defrost control parameter.

1. INTRODUCTION

Light commercial refrigerators are widely used to preserve, store and sell fresh or frozen food products in business locations. Although this class of equipment has become essential for the food supply chain, they are also responsible for significant energy consumption and associated carbon dioxide emissions. These systems are generally designed with air curtains or subjected to frequent door openings which allow air and water vapour to infiltrate in the refrigerated space. When the evaporator operates under freezing temperatures, this extra amount of moisture accumulates as frost on the heat exchanger surface. The frost layer penalizes the evaporator performance by increasing its thermal resistance and reducing the fan air flow rate (Da Silva *et al.* 2010). As a result, the evaporating temperature progressively reduces to remove the thermal load, until the coil is defrosted to recover its original performance.

Stoecker (1957) carried out one of the first investigations into the frost formation on finned tube evaporators and identified a relation between the accumulation of frost and the decrease in the air flow rate, indicating the increase in the evaporator air pressure drop as a parameter to control the defrost process. After this, a substantial number of numerical and experimental studies have been reported on frosting of evaporator coils (Tassou *et al*., 1987; Kondepudi *et al*., 1987; Rite *et al*., 1991; Seker *et al*., 2004; Zhang *et al*., 2009) but only a small number have involved coils of commercial display cabinets. Tassou *et al.* (2001) investigated the frost formation and defrosting process of commercial display cabinets operating under different ambient conditions. The authors pointed out that the number of defrost cycles is generally overestimated, resulting in energy loss and excessive product temperature variations. They also concluded that the ambient air enthalpy can be used as an efficient defrosting control parameter. Later, Aljuwayhel *et al*. (2008) conducted an experimental study of frost formation on industrial evaporators and proposed an iterative procedure to obtain an optimal defrost control based on the measurement of the drained water during the melting period.

However, all the previously mentioned methods, proposed to control the defrost process, are very difficult to be implemented in small display cabinets due to cost considerations. Hence, in this study, special attention will be placed on the parameters that can be easily employed to establish a relation with the refrigeration system performance for initiation of defrost on demand.

2. EXPERIMENTAL WORK

2.1 Refrigeration system

A serve-over cabinet was equipped with different transducers and its performance investigated in an environmental test chamber at controlled conditions of ambient temperature, relative humidity and air velocity. Figure 4 shows the cabinet and the main air flow direction inside the refrigerated space. As illustrated, the evaporator was located below the base shelve and the air flow propelled by fans, represented by the yellow arrows, was divided in two main streams at the evaporator exit. One of this streams moves upwards forming an air curtain, whereas the other moves directly to the base shelf which was designed to operate at lower temperatures. The product thermal load was simulated by thirty plastic containers filled with water and two test packages with thermal characteristics corresponding to lean beef. The temperature of these thermal loads was measured during the tests. In addition, the external air infiltration, indicated by the blue dotted arrow in Fig. 1, also contributed to the sensible and latent thermal load and it was the main source of humidity for the frost formation process during the experiments.

Figure 2 illustrates the main components of the refrigeration circuit and the transducers used to evaluate the evaporator performance. The system was equipped with a reciprocating compressor (COMP) of 12.87 cm^3 volumetric displacement operating with refrigerant R-404a. The refrigerant control device was a thermostatic expansion valve (TV) and its remote bulb was installed at the exit coil position. The condenser (COND) and the evaporator (EVAP) operated under air forced convection by means of one and three axial fans (FAN), respectively. An off-cycle defrost approach was implemented by means a PID controller, which periodically turned off the compressor with the evaporator fans left on during the off-cycle defrosting process.

The refrigerant mass flow rate was measured by a coriolis-type transducer (MFM) with a maximum uncertainty of ±0.2 kg/h. This transducer was installed after the liquid receiver (LR) and a sigh glass (SG) for liquid flow visualisation purposes. The high and low side pressures were measured by two absolute pressure transducers (PT) installed before the compressor and the thermostatic valve, respectively. The maximum uncertainty for the pressure measurement was ±10 kPa. The relative humidity was measured in the inlet and exit evaporator position by two capacitive humidity transducers (RH) that provided a maximum uncertainty of ±1.5%. The air and the refrigeration system temperatures were measured by T-type thermocouples (TC), with a maximum uncertainty of ±0.2°C.

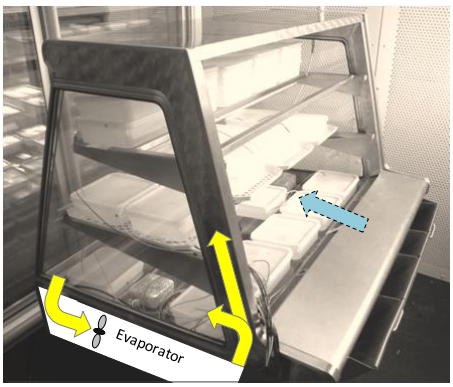

Figure 1. Over serve cabinet and the air flow direction

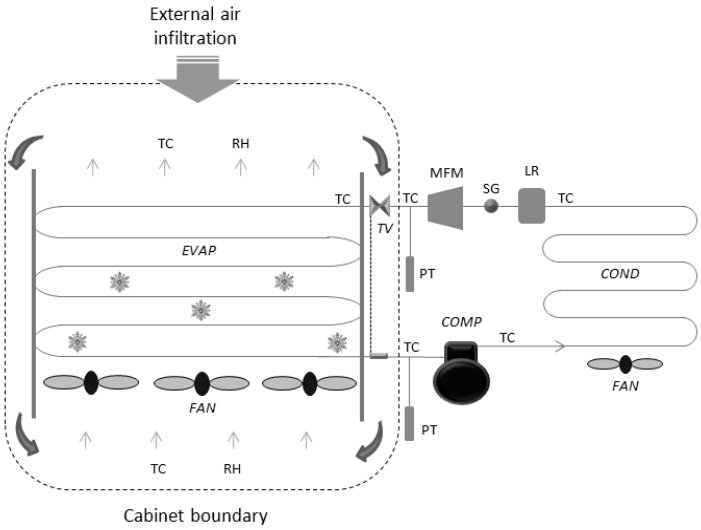

Figure 2. Schematic of the refrigeration circuit and instrumentation

The evaporator was a finned circular tube cross-flow heat exchanger, as showed in Fig. 3. It was installed in a counter-flow configuration, in such way that the refrigerant exits from the front side of the evaporator coil (i.e., the air inlet side). The wavy-fins are made of aluminum alloy with thickness of 0.3 mm and a fin density of 1.2 fins/cm. The tubes are made of cupper with an outer diameter of 13 mm. The external dimensions of the front face, not including the end turns, are 750 x 75 mm and the length of the evaporator in

the direction of the air flow is 395 mm. The tubes are arranged in twelve staggered rows with two tubes each. The longitudinal (parallel to the air flow) and transverse tube pitches are 32 mm and 38 mm, respectively. As can be seen in Fig. 3, five thermocouples (TC) were installed at different positions along the coil in order to measure the refrigerant temperature profile.

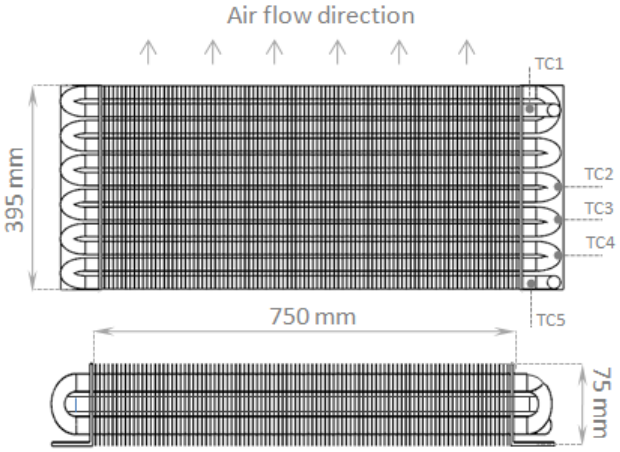

Figure 3. Schematic view of the evaporator under analysis

2.2 Data processing

The mass and energy balance were applied on the refrigerant and air sides to calculate the evaporator total cooling capacity (q), sensible (q_s) and latent (q_l) heat transfer rates, as follows:

$$q = m_r \left(h_2 - h_1 \right) \tag{1}$$

$$q = q_s + q_l = m_a c_{p,a} \left(T_{a,1} - T_{a,2} \right) + m_a \left(\omega_1 - \omega_2 \right) L \tag{2}$$

where m_r is the refrigerant mass flow rate [kg/s], h is the refrigerant enthalpy [J/kg], indices 1 and 2 refer to inlet and exit evaporator position, respectively, m_a is the air mass flow rate [kg/s], $c_{p,a}$ is the air specific heat at constant pressure [J $kg^{-1}°C^{-1}$], T_a is the air temperature [°C], ω is the humidity ratio [kg_v kg_a^{-1}] and L is the latent heat of desublimation [J kg^{-1}]. The mass of frost accumulated over time, M_f, was calculated from,

$$M_f = \int m_a \left(\omega_1 - \omega_2 \right) dt \tag{3}$$

2.3 Operational conditions

The tests were carried out following the recommendations of ISO 23953-2 (2005). Table 1 shows the internal test chamber conditions and the average refrigerant temperature at evaporator inlet used during the experiments. The air movement inside the chamber was parallel to the plane of the cabinet display opening. The ambient air velocity was fixed at around 0.2 m/s, while the temperature and relative humidity were varied to analyze their effect on the measured variables and the system energy performance. Moreover, the time interval between the beginning of two defrost cycles was set at 6 hours, with a defrost duration of 20 minutes. The data were collected after two defrost cycles.

Table 1. Summary of the experimental conditions

Test	u_{amb} [m/s]	ϕ_{amb}[%]	T_{amb} [°C]	ω_{amb} [g_v/kg_a]	$T_{ev,1}$ [°C]
1	0.2	60	25.0	11.9	-8.5
2	0.2	60	21.0	9.3	-11.5
3	0.2	45	25.0	8.9	-10.0
4	0.2	45	21.0	6.9	-12.0

3. RESULTS AND DISCUSSION

Figure 4 shows the influence of the operational parameters on the accumulated mass of frost, obtained from the air-side mass balance. In all investigated conditions, a nearly linear relation was observed between the accumulated mass of frost and time. An increase of the frost deposition rate with the ambient humidity ratio can also be seen from the data in Table 1. For instance, tests #1 and #4 yield a final mass of frost of 2.5 kg and 1.75 kg, respectively, which represents a total difference of 43%. The initial and final appearance of the air inlet side of the evaporator can be compared in Fig. 5, which shows a significant amount of the original free space occupied by the frost layer. In this situation, test #1, the ambient humidity ratio was of 11.9 g_v/kg_a and the evaporating temperature -8.5°C.

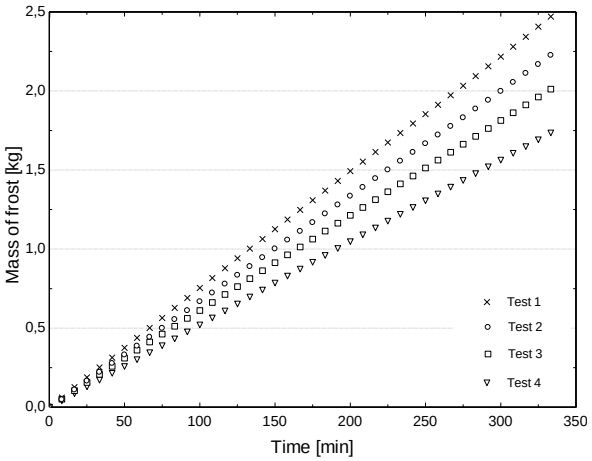

Figure 4. Accumulated mass of frost for different operating conditions

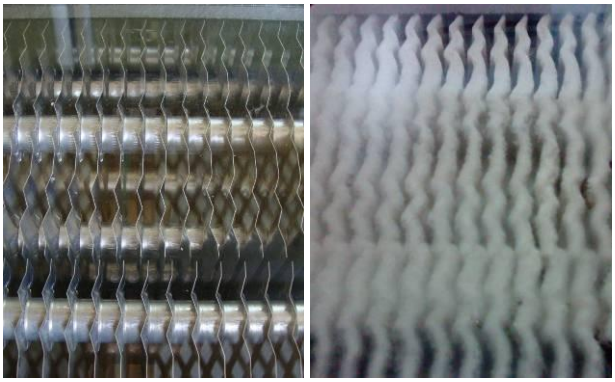

(a) (b)

Figure 5. Comparison between initial(a) and final(b) visualization of the evaporator coil for test #1

Figure 6 illustrates the temporal variation of the evaporator pressure for all test conditions. As can be seen the evaporator pressure decreases over time resulting in lower evaporator temperatures. A comparison between the tested conditions shows that the average evaporating pressure is affected by the environment conditions and increases with the ambient temperature and the relative humidity. In addition, it is also observed that the average pressure reduction is more significant for tests 1# and 2# than for tests 3# and 4#, respectively, which were carried out at lower humidity ratios. As a result of pressure changes, similar trends were observed for the refrigerant mass flow rate behaviour that is illustrated in Fig. 7. Again, a faster reduction was observed for high humidity ratio conditions. The influence of the higher air moisture content is clear for tests #2 and #4, carried out at the same ambient temperature, that show the variation in the refrigerant mass flow rate and the changeover that takes place in the values after approximately 250 min.

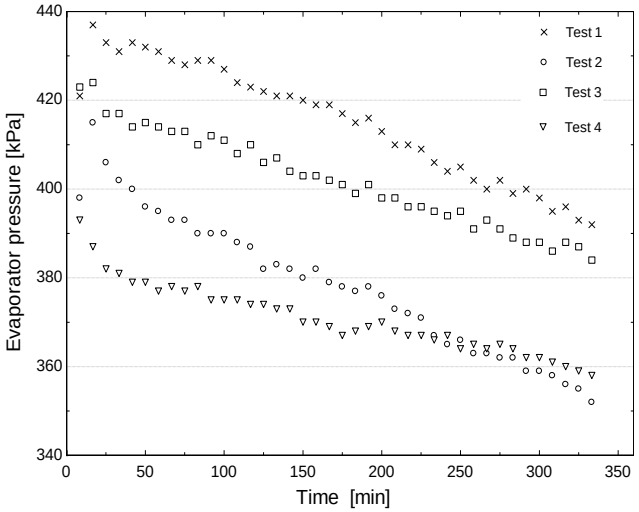

Figure 6. Evaporator pressure variation for different operating conditions

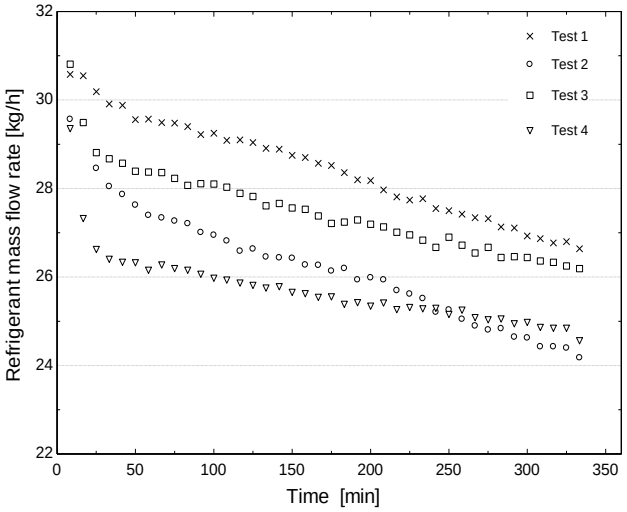

Figure 7. Refrigerant mass flow rate variation for different operating conditions

An assessment of the combined effect of the mass of frost and system parameters on the cooling capacity of the coil is illustrated in Fig. 8. From this graph it is possible to see that the cooling capacity steadily decreases over time. Although tests #1 and #2 initiate with higher cooling capacities they decrease faster at 21 W/h, while the rate of decrease for tests #3 and #4 was 14 W/h and 10 W/h, respectively. It is apparent from these results that the reduction in the cooling capacity increases with the ambient humidity ratio, indicating the importance of the air moisture content control. Moreover, for test #1, the latent heat part of the total cooling capacity was evaluated as 43%, showing that a significant amount of the cooling capacity does not contribute to the reduction in the refrigerated space temperature. Figure 9 shows the average product temperature for the base shelf of the cabinet. As can be seen, the temperature increases with the ambient air temperature and relative humidity (see Tab. 1). Although the average product temperature initially decreases, this trend is reversed for tests #1 and #3 after 225 and 300 min, respectively, indicating an insufficient cooling capacity due to the negative effects of frost on system performance.

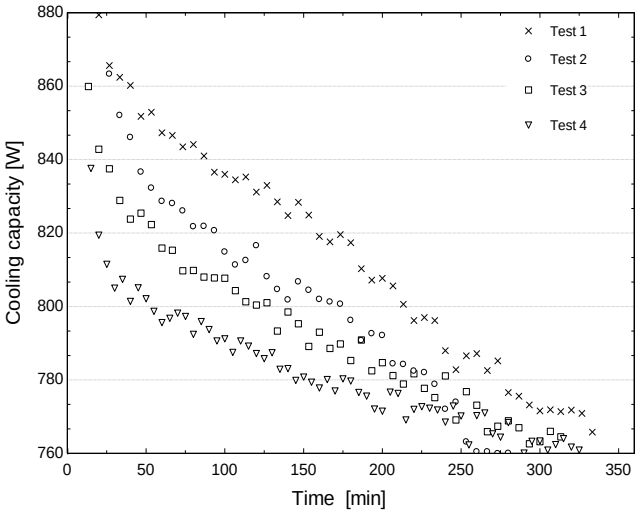

Figure 8. Cooling capacity variation for different operational conditions

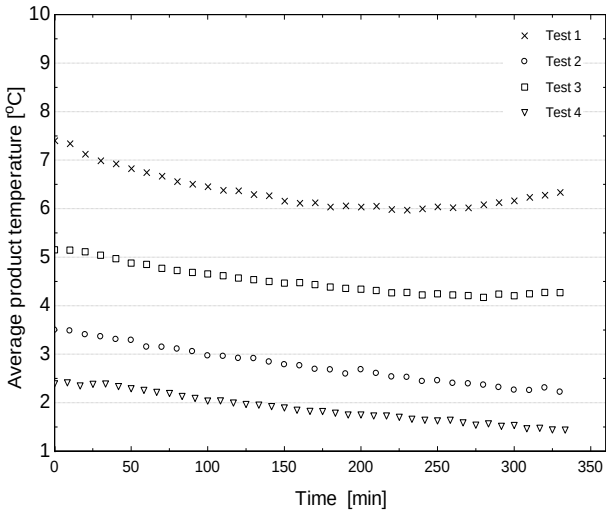

Figure 9. Product temperature variation for different operational conditions

The reduction in the cooling capacity was also analysed in order to identify its relation to different parameters. Because the convenience of defrost strategies based on temperature measurement, the variation of this property was investigated in detail. Figure 10 compares the temperature variation, measured at different positions on the coil surface (see Fig. 3), with the cooling capacity for test #1. As can be seen, the coil temperature and the cooling capacity have decreasing trends. It is also observed that the evaporator is flooded with liquid refrigerant until TC3 position. TC5 indicates the temperature of the superheated refrigerant at the evaporator outlet. The fast reduction observed after 150 minutes for TC4 indicates the advance of the liquid front inside the coil. Moreover, the beginning of the defrost process is indicated by the whole evaporator temperature increases after 340 min. Similar trends were observed for other test conditions presented in Table 1.

The degree of correlation between the cooling capacity and the coil temperature, measured at different positions, was assessed by the coefficient of determination (r^2). Using a linear regression, the higher r^2 values were obtained with the temperatures measured at TC5 position. Figure 11 shows the relation between the exit refrigerant temperature reduction ($T_o - T_t$), measured at TC5 position, and the percentage cooling capacity reductions. For all investigated conditions, a maximum difference of ±2.5% was observed between the data points and the single fitted curve , $y = 1.8x + 3.2$, where y represents the cooling capacity reduction and x is the exit temperature reduction. Therefore, these results show the potential application of the exit refrigerant temperature variation as a control parameter that can reflect well the system performance. This strategy not only can determine the beginning of the defrost process based on the reduction of the cooling capacity, but can also be implemented at relatively low cost compared to defrost controls based on measurements of other parameters.

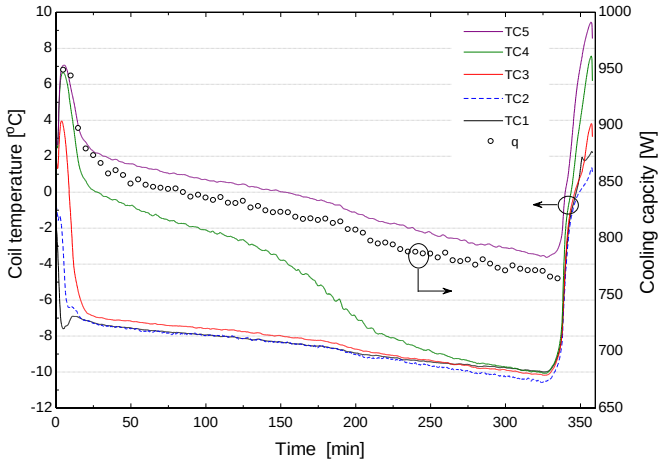

Figure 10. Comparison between coil temperature and cooling capacity for test #1

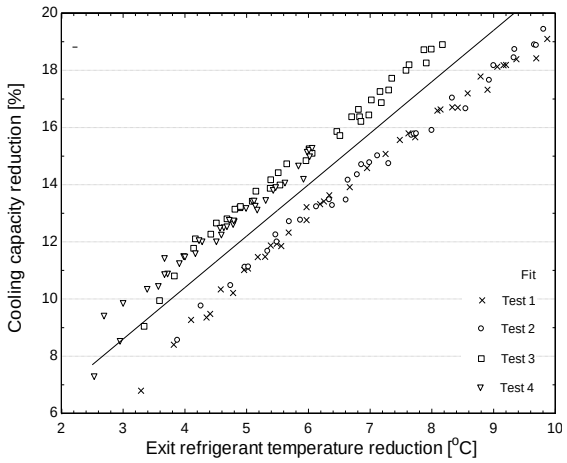

Figure 11. Relation between exit refrigerant temperature reduction and cooling capacity

4. FINAL REMARKS

A serve-over counter cabinet was instrumented and tested in an environmental test chamber at controlled conditions of ambient temperature and relative humidity. The mass and energy balance were carried out on the evaporator to evaluate the cooling capacity and the mass of frost accumulated on the coil surface. For the entire set of tests, it was observed that the evaporator pressure and the refrigerant mass flow rate increase with the ambient temperature and relative humidity, and also decrease faster over time with high ambient air moister contents. In addition, it was observed that the accumulated mass of frost and the rate of cooling capacity reduction increase with the ambient air humidity, reinforcing the importance of reduction of the latent infiltration load. A linear relationship between the reduction in the cooling capacity and exit refrigerant temperature variation has been identified which predicts the decrease in the performance with a maximum difference of ±2.5% between single fitted curve and the data points. The results suggests that this kind of correlation can be conveniently used for defrost initiation and implementation of defrost on demand to reduce energy consumption and improve product quality.

5. ACKNOWLEDGEMENTS

This study was carried out at the School of Design and Engineering - Brunel University. The financial support from the Department for Environment, Food and Rural Affairs (Defra) is duly acknowledged. Thanks are also addressed to the CNPq Council of the Ministry for Science and Technology of Brazil. The authors would also like to acknowledge the valuable technical support from Mr INyoman Suamir and Mr Costas Xanthos.

6. REFERENCES

Aljuwayhel NF, Reindl DT, Klein SA, Nellis GF, 2008, Experimental investigation of the performance of industrial evaporator coils operating under frosting conditions, International Journal of Refrigeration, 31(1): 98-106.

Chen H, Thomas L, Besant, RW. 2003, Fan supplied heat exchanger fin performance under frosting conditions, International Journal of Refrigeration, 26: 140-149.

Da Silva DL, Hermes CJL, Melo C. 2010, Experimental study of frost accumulation on fan-supplied tube-fin evaporators, Applied Thermal Engineering, 31: 1013-1020.

ISO 23953-2. 2005, Refrigerated display cabinets - Part 2: Classification, requirements and test conditions, International Organization for Standardization.

Kondepudi SN, O'Neal DL. 1987, The effect of frost growth on extended surface heat exchanger performance: A review, ASHRAE Transactions, 93: 258-274.

Rite RW, Crawford RR. 1991, The effect of frost accumulation on the performance of domestic refrigerator-freezer finned-tube evaporator coils, ASHRAE Transactions, 97(2): 428-437.

Seker D, Karatas H, Egrican N. 2004, Frost formation on fin-and-tube heat exchangers. Part I – Modeling of frost formation on fin-and-tube heat exchangers, International Journal of Refrigeration, 27: pp: 367-374.

Stoecker WF. 1957, How frost formation on coils affects refrigeration systems, Refrigerating Engineering, 65(2).
Tassou SA, Marquand CJ. 1987, Effect of evaporator frosting and defrosting on the performance of air-to-water heat pumps, Applied Energy, 28: 19-33.
Tassou SA, Datta D, Marriott D. 2001, Frost formation and defrost control parameters for open multideck refrigerated food display cabinets, Proceedings of the Institution of Mechanical Engineers, Part A: Journal of Power and Energy, 215(2): 213:222.
Zhang, P, Hrnjak PS. 2009, Air-side performance evaluation of three types of heat exchangers in dry, wet and periodic frosting conditions, International Journal of Refrigeration, 32: 911-921.

7. NOMENCLATURE

Roman

c_p	specific heat at constant pressure [J kg^{-1} K^{-1}]
h	refrigerant enthalpy [J kg^{-1}]
m	mass flow rate [kg s^{-1}]
M	accumulated mass of frost [kg]
L	frost latent heat of desublimation [J kg^{-1}]
q	cooling capacity [W]
T	temperature [°C]
t	time [s]
u	air velocity [m s^{-1}]

Greek

ϕ	relative humidity [%]
ω	humidity ratio [kg$_v$ kg$^{-1}{}_a$]

Subscripts

a	air
amb	ambient
ev	evaporator
f	frost
l	latent
o	initial time
r	refrigerant
s	sensible
t	moment time
v	water vapor
1	inlet
2	exit